



1 **Indirect contributions of global fires to surface ozone through**  
2 **ozone-vegetation feedback**

3

4 **Yadong Lei<sup>1,2</sup>, Xu Yue<sup>3\*</sup>, Hong Liao<sup>3</sup>, Lin Zhang<sup>4</sup>, Yang Yang<sup>3</sup>, Hao Zhou<sup>1,2</sup>,**  
5 **Chenguang Tian<sup>1,2</sup>, Cheng Gong<sup>2,5</sup>, Yimian Ma<sup>1,2</sup>, Lan Gao<sup>1,2</sup>, Yang Cao<sup>1,2</sup>**

6 <sup>1</sup>Climate Change Research Center, Institute of Atmospheric Physics, Chinese  
7 Academy of Sciences, Beijing, 100029, China

8 <sup>2</sup>University of Chinese Academy of Sciences, Beijing, 100029, China

9 <sup>3</sup>Jiangsu Key Laboratory of Atmospheric Environment Monitoring and Pollution  
10 Control, Collaborative Innovation Center of Atmospheric Environment and  
11 Equipment Technology, School of Environmental Science and Engineering, Nanjing  
12 University of Information Science & Technology (NUIST), Nanjing, 210044, China

13 <sup>4</sup>Laboratory for Climate and Ocean–Atmosphere Studies, Department of Atmospheric  
14 and Oceanic Sciences, School of Physics, Peking University, Beijing, 100871, China

15 <sup>5</sup>State Key Laboratory of Atmospheric Boundary Layer Physics and Atmospheric  
16 Chemistry (LAPC), Institute of Atmospheric Physics, Chinese Academy of Sciences,  
17 Beijing, 100029, China

18 *Correspondence to:* Xu Yue ([yuexu@nuist.edu.cn](mailto:yuexu@nuist.edu.cn))

19

20

21

22



23 **Abstract:** Fire is an important source of surface ozone ( $O_3$ ), which causes damage to  
24 vegetation and reduces stomatal conductance. Such processes can feed back to inhibit  
25 dry deposition and indirectly enhance surface  $O_3$ . Here, we apply a fully coupled  
26 chemistry-vegetation model to estimate the indirect contributions of global fires to  
27 surface  $O_3$  through  $O_3$ -vegetation feedback during 2005-2012. Fire emissions directly  
28 increase the global mean annual  $O_3$  by 1.2 ppbv (5.0%) with a maximum of 5.9 ppbv  
29 (24.4%) averaged over central Africa by emitting substantial number of precursors.  
30 Considering  $O_3$ -vegetation feedback, fires additionally increase surface  $O_3$  by 0.5  
31 ppbv averaged over the Amazon in October, 0.3 ppbv averaged over southern Asia in  
32 April, and 0.2 ppbv averaged over central Africa in April. During extreme  
33  $O_3$ -vegetation interactions, such feedback can rise to  $>0.6$  ppbv in these fire-prone  
34 areas. Moreover, large ratios of indirect-to-direct fire  $O_3$  are found in eastern China  
35 (3.7%) and the eastern U.S. (2.0%), where the high ambient  $O_3$  causes strong  
36  $O_3$ -vegetation interactions. With likelihood of increasing fire risks in a warming  
37 climate, fires may promote surface  $O_3$  through both direct emissions and indirect  
38 chemistry-vegetation feedbacks. Such indirect enhancement will cause additional  
39 threats to public health and ecosystem productivity.

40

41 **Keywords:** fires, surface ozone, dry deposition, ozone-vegetation feedback

42

43

44



## 45 **1 Introduction**

46 Fire plays an important role in disturbing the terrestrial carbon budget  
47 (Bond-Lamberty et al., 2007; Amiro et al., 2009; Turetsky et al., 2011; Yue and Unger,  
48 2018). Global fires directly emit 2-3 Pg (1 Pg =  $10^{15}$  g) carbon into the atmosphere  
49 every year (van der Werf et al., 2010). Moreover, fires contribute to the production of  
50 tropospheric ozone ( $O_3$ ) by emitting substantial number of precursors (Cheng et al.,  
51 1998; Kita et al., 2000; Oltmans et al., 2010; Jaffe et al., 2013; Lu et al., 2016).  
52 Globally, fires account for 3-5% of the total tropospheric  $O_3$  (Bey et al., 2001; Ziemke  
53 et al., 2009; Jaffe and Wigder, 2012). Regionally, the influence of fires on  $O_3$   
54 production is dependent on mixing with urban emissions (Jaffe et al., 2004; Singh et  
55 al., 2010). In some areas, fires can enhance surface  $O_3$  by 10-30 ppbv through  
56 emissions of  $NO_x$  and VOCs (McKeen et al., 2002; Pfister et al., 2008; Yue and Unger,  
57 2018). Model simulations project that future wildfire activity will likely increase due  
58 to global warming, suggesting an increased risk of surface  $O_3$  from wildfires (Amiro  
59 et al., 2009; Balshi et al., 2009; Wang et al., 2016; Yue et al., 2017).

60

61 Tropospheric  $O_3$  is a toxic air pollutant with detrimental effects on vegetation (Yue  
62 and Unger, 2014). Plant stomatal uptake of  $O_3$  decreases both chlorophyll and  
63 Rubisco contents and increases the deformity rate of chloroplasts (Booker et al., 2007;  
64 Akhtar et al., 2010; Inada et al., 2012), which further reduces the leaf area index (LAI)  
65 and gross primary productivity (GPP) of ecosystems (Karnosky et al., 2007;  
66 Ainsworth et al., 2012). Modeling studies estimated that fire-induced  $O_3$  reduces



67 global GPP by 0.7% with regional maximum reductions of >4.0% over central Africa  
68 (Yue and Unger, 2018). In turn, vegetation influences both the sources and sinks of O<sub>3</sub>  
69 through biogeochemical and biogeophysical feedbacks (Curci et al., 2009; Heald and  
70 Geddes, 2016; Fitzky et al., 2019). Emissions from biomass burning generate a large  
71 amount of O<sub>3</sub> precursors (Jaffe and Wigder, 2012; Lu et al., 2016). Moreover,  
72 vegetation acts as an important sink for tropospheric O<sub>3</sub> through stomatal uptake  
73 (Wesely and Hicks, 2000; Val Martin et al., 2014). Globally, stomatal uptake  
74 contributes to 40-60% of the canopy total O<sub>3</sub> deposition (Fowler et al., 2009).

75

76 Interactions between air pollution and terrestrial ecosystems remain challenging due  
77 to limited process-based knowledge and the separate development of chemistry and  
78 vegetation models (He et al., 2020). At present, the feedbacks from O<sub>3</sub>-damaging  
79 vegetation on O<sub>3</sub> have only been examined by three papers. By implementing  
80 steady-state O<sub>3</sub>-induced LAI changes into a chemical transport model, Zhou et al.  
81 (2018) quantified the influences of O<sub>3</sub>-vegetation feedback and found that O<sub>3</sub>-induced  
82 damage to LAI can enhance O<sub>3</sub> by up to 3 ppbv in the tropics, eastern North America,  
83 and southern China. Moreover, plant stomatal conductance may decrease to prevent  
84 excessive O<sub>3</sub> from entering plants (Manninen et al., 2003; Wittig et al., 2009).  
85 Consequently, surface O<sub>3</sub> may increase due to reduced dry deposition (Val Martin et  
86 al., 2014; Lin et al., 2019). Sadiq et al. (2017) implemented a parameterization of O<sub>3</sub>  
87 vegetation damage into a climate model and quantified online O<sub>3</sub>-vegetation coupling.  
88 Simulation results showed that surface O<sub>3</sub> can be enhanced by up to 4-6 ppbv over



89 Europe, North America, and China mainly because of reduced dry deposition velocity  
90 following O<sub>3</sub> damage. Similarly, Gong et al. (2020) used a fully coupled  
91 chemistry-carbon-climate global model and found that O<sub>3</sub>-induced inhibition of  
92 stomatal conductance can increase surface O<sub>3</sub> by 1.4-2.1 ppbv in eastern China and  
93 1.0-1.3 ppbv in western Europe. All studies revealed strong positive O<sub>3</sub>-vegetation  
94 feedback to surface O<sub>3</sub>, although the magnitudes are different due to discrepancies in  
95 O<sub>3</sub> damaging schemes, as well as differences in the climate models.

96

97 Many studies have quantified the direct contributions of fires to tropospheric O<sub>3</sub>  
98 (Martin et al., 2006; Pfister et al., 2006; Ziemke et al., 2009; Yokelson et al., 2011;  
99 Jaffe and Wigder, 2012; Larsen et al., 2018; Yue and Unger, 2018). However, the  
100 feedback of fire-induced O<sub>3</sub> vegetation damage to surface O<sub>3</sub> remain unquantified.  
101 Here, we apply a fully coupled chemistry-vegetation model (GEOS-Chem-YIBs,  
102 hereafter referred to as GC-YIBs) to examine the indirect contributions of fires to  
103 surface O<sub>3</sub>. Fire-induced O<sub>3</sub> affects plant photosynthesis and stomatal conductance. In  
104 turn, predicted changes in LAI and canopy stomatal conductance influence both the  
105 sources and sinks of tropospheric O<sub>3</sub>. Such O<sub>3</sub>-vegetation interactions result in  
106 additional enhancement in surface O<sub>3</sub> caused by fire emissions (Fig. 1). Section 2  
107 describes the GC-YIBs model and sensitivity experiments conducted in this study.  
108 Section 3 quantifies the feedbacks of fire-induced O<sub>3</sub> vegetation damage on surface  
109 O<sub>3</sub> concentrations. The last section summarizes the findings and discusses the  
110 uncertainties.



111

## 112 **2 Materials and Methods**

### 113 **2.1 The GC-YIBs model**

114 GC-YIBs is a coupled chemistry-vegetation model developed by implementing the  
115 Yale Interactive terrestrial Biosphere (YIBs) model into GEOS-Chem version 12.0.0  
116 (Lei et al., 2020). GEOS-Chem is a widely used global 3-D chemical transport model  
117 (CTM) for simulating atmospheric composition and air quality (Yue et al., 2015; Yan  
118 et al., 2018; David et al., 2019; Lu et al., 2019). This model uses a detailed  
119 HO<sub>x</sub>-NO<sub>x</sub>-VOC-O<sub>3</sub>-halogen-aerosol tropospheric chemistry to simulate tropospheric  
120 O<sub>3</sub> fluxes (Barret et al., 2016; Gong and Liao, 2019), while a simplified linearized  
121 Linoz chemistry mechanism is applied to simulate stratospheric O<sub>3</sub> (McLinden et al.,  
122 2000). Aerosols simulated in GEOS-Chem include secondary inorganic aerosols,  
123 secondary organic aerosols, primary organic aerosols, black carbon, dust, and sea salt  
124 (Dang and Liao, 2019; Li et al., 2019). The gas-aerosol partitioning of the  
125 sulfate–nitrate–ammonium system is computed by the ISORROPIA v2.0  
126 thermodynamic equilibrium model (Fountoukis and Nenes, 2007). The atmospheric  
127 emissions from different sources, regions, and species on a user-defined grid are  
128 calculated through the online Harvard NASA Emissions Component (HEMCO)  
129 module (Keller et al., 2014). HEMCO is highly customizable in that it can  
130 automatically combine, overlay, and update emission inventories and scale factors  
131 specified by the users. In general, the GEOS-Chem model overestimates summer  
132 surface O<sub>3</sub> concentrations in the eastern U.S. and China (Zhang et al., 2011; Travis et



133 al., 2016; Schiferl and Heald, 2018).

134

135 YIBs is a vegetation model designed to dynamically simulate the changes in LAI and  
136 tree height based on carbon assimilation, respiration, and allocation processes (Yue  
137 and Unger, 2015). The model computes carbon uptake for 9 vegetation types,  
138 including evergreen needleleaf forest, deciduous broadleaf forest, evergreen broadleaf  
139 forest, shrubland, tundra, C<sub>3</sub>/C<sub>4</sub> grasses, and C<sub>3</sub>/C<sub>4</sub> crops. The YIBs model applies a  
140 well-established Michaelis–Menten enzyme kinetics scheme to compute the leaf  
141 photosynthesis for C<sub>3</sub> and C<sub>4</sub> plants (Farquhar et al., 1980; Von Caemmerer and  
142 Farquhar, 1981). The leaf stomatal conductance was calculated based on the model of  
143 Ball and Berry (Baldocchi et al., 1987). The Spitters (1986) canopy radiative transfer  
144 scheme is used to separate light use processes for sunlit and shaded leaves. The LAI  
145 and carbon allocation schemes are from the TRIFFID model (Clark et al., 2011).  
146 Previous studies have shown that the YIBs model has good performance in simulating  
147 the spatial pattern and temporal variability of GPP and LAI based on site observations  
148 and satellite products (Yue and Unger, 2015, 2018).

149

150 The GC-YIBs model links atmospheric chemistry and vegetation in a two-way  
151 coupling. As a result, changes in chemical components or vegetation will  
152 simultaneously feed back to influence the other systems. In this study, the GC-YIBs  
153 model is driven with the meteorological fields from the Modern-Era Retrospective  
154 analysis for Research and Applications, version 2 (MERRA2) with a horizontal



155 resolution of 4° latitude by 5° longitude, as well as 47 vertical layers from the surface  
156 to 0.01 hPa. Within GC-YIBs, the online-simulated surface O<sub>3</sub> in GEOS-Chem affects  
157 photosynthesis and canopy stomatal conductance; in turn, the online-simulated  
158 vegetation parameters, such as LAI and stomatal conductance, in YIBs, affect both the  
159 sources and sinks of O<sub>3</sub> by altering precursor emissions and dry deposition at the  
160 1-hour integration time step. An earlier study evaluated the GC-YIBs model and  
161 showed good performance in simulating surface O<sub>3</sub>, GPP, LAI, and O<sub>3</sub> dry deposition  
162 (Lei et al., 2020).

163

## 164 **2.2 Scheme of O<sub>3</sub> vegetation damage**

165 The GC-YIBs model calculates the impacts of O<sub>3</sub> exposure on photosynthesis based  
166 on a semi-mechanistic scheme (Sitch et al., 2007):

$$167 \quad A' = \alpha \cdot A \quad (1)$$

168 where  $A'$  and  $A$  represent the O<sub>3</sub>-damaging and original leaf photosynthesis,  
169 respectively. The O<sub>3</sub> damage factor is represented by  $\alpha$ ; O<sub>3</sub> can cause damage to  
170 photosynthesis only if  $\alpha < 1$ . The factor  $\alpha$  is calculated as a function of excessive O<sub>3</sub>  
171 flux and damaging sensitivity coefficient ( $\beta$ ):

$$172 \quad \alpha = -\beta \cdot \max(F_{O_3} - T_{O_3}, 0) \quad (2)$$

173 The coefficient  $\beta$  can have two values for each vegetation type (Table S1), indicating  
174 low to high O<sub>3</sub> damaging sensitivities (Sitch et al., 2007).  $T_{O_3}$  represents the O<sub>3</sub> flux  
175 threshold, reflecting the O<sub>3</sub> tolerance of different vegetation types.  $F_{O_3}$  represents the  
176 stomatal O<sub>3</sub> flux and is calculated based on ambient  $[O_3]$ , aerodynamic resistance





177 ( $r_a$ ), boundary layer resistance ( $r_b$ ) and stomatal resistance ( $r_s$ ):

$$178 \quad F_{O_3} = \frac{[O_3]}{r_a + r_b + k \cdot r_s'} \quad (3)$$

179 Here  $k$  represents the ratio of leaf resistance for  $O_3$  to leaf resistance for water vapor.

180 Parameters  $r_a$  and  $r_b$  are calculated by the GEOS-Chem model.  $O_3$ -damaging leaf

181 photosynthesis ( $A'$ ) is then integrated over all canopy layers to generate  $O_3$ -damaging

182 GPP:

$$GPP' = \int_0^{LAI} A' dL$$

183 The  $O_3$ -damaging stomatal resistance ( $r_s'$ ) is calculated based on the model of Ball

184 and Berry (Baldocchi et al., 1987):

$$185 \quad \frac{1}{r_s'} = g_s' = m \frac{A'_{net} \cdot RH}{c_s} + b \quad (4)$$

186 where  $m$  and  $b$  represent the slope and intercept of empirical fitting to the Ball-Berry

187 stomatal conductance equation, respectively.  $A'_{net}$  represents  $O_3$ -damaging net leaf

188 photosynthesis,  $RH$  represents the relative humidity and  $c_s$  is the ambient  $CO_2$

189 concentration. Previous studies have shown that this scheme within the framework of

190 YIBs can reasonably capture the response of GPP and stomatal conductance to

191 surface  $[O_3]$  based on hundreds of global observations (Yue et al., 2016; Yue and

192 Unger, 2018).

193

### 194 **2.3 Fire emissions**

195 Fire Inventory from NCAR (FINN) version 1.5 is used by GC-YIBs to simulate

196 fire-induced perturbations in  $O_3$ . FINN provides daily global emissions of many

197 chemical species from open biomass burning at a resolution of  $1 \text{ km}^2$  (Wiedinmyer et



198 al., 2011). The inventory estimates fire locations and biomass burned using satellite  
199 observations of active fires and land cover, together with emission factors and fuel  
200 loadings. For each land type, emission factors for different gaseous and particulate  
201 species are taken from measurements (Andreae and Merlet, 2001; Andreae and  
202 Rosenfeld, 2008; Akagi et al., 2011). Daily fire emissions for 2002-2012 are available  
203 at <http://bai.acom.ucar.edu/Data/fire/>. In GC-YIBs, all biomass burning emissions are  
204 emitted into the atmospheric boundary layer. The FINN inventory has been widely  
205 used in regional and global chemical transport models (e.g., WRF-Chem and  
206 GEOS-Chem) to quantify the impacts of fires on air quality and weather (Jiang et al.,  
207 2012; Nuryanto, 2015; Vongruang et al., 2017; Brey et al., 2018; Watson et al., 2019).

208

#### 209 **2.4 Site-level measurements**

210 Measurements of surface [O<sub>3</sub>] in the U.S. are provided by Air Quality System (AQS,  
211 <https://www.epa.gov/aqs>), those over Europe are provided by European Monitoring  
212 and Evaluation Programme (EMEP, <https://emep.int>). The observed [O<sub>3</sub>] at Manaus,  
213 Tg Malim, and Welgegund sites are from earlier studies (Ahamad et al., 2014; Laban  
214 et al., 2018; Pope et al., 2020).

215

#### 216 **2.5 Model simulations**

217 In this study, eight simulations (Table 1) are performed to examine both the direct and  
218 indirect contributions of fires to surface O<sub>3</sub>. These simulations can be divided into two  
219 main groups:



220 1. CTRL\_FIRE and CTRL\_NOFIRE are the control runs using the same emissions  
221 except that the latter omits fire emissions. These runs calculate and output offline  
222 O<sub>3</sub> damage, which decreases instantaneous leaf photosynthesis but does not feed  
223 back to affect plant growth and O<sub>3</sub> dry deposition.

224 2. O3CPL\_FIRE and O3CPL\_NOFIRE are the sensitive experiments that consider  
225 online coupling between O<sub>3</sub> and vegetation. These runs include online O<sub>3</sub> damage  
226 to plant photosynthesis, which feeds back to affect both vegetation and air  
227 pollution. The two simulations apply the same emissions, except that the latter  
228 omits fire emissions.

229

230 For each of these four configurations, two runs are conducted with either high (HS) or  
231 low (LS) O<sub>3</sub> damaging sensitivities. All simulations are performed from 2002-2012  
232 using the GC-YIBs model driven by MERRA2 meteorological fields. The first 3 years  
233 are used as spin up, and the results of the last 8 years are analyzed. For the same  
234 configurations, the results from low and high O<sub>3</sub> damaging sensitivities are averaged.

235 The differences between CTRL\_NOFIRE and O3CPL\_NOFIRE represent the surface  
236 O<sub>3</sub> enhancements through O<sub>3</sub>-vegetation feedback without fire emissions. The  
237 differences between CTRL\_FIRE and CTRL\_NOFIRE, named O3OFF, represent the  
238 direct contributions of fires to surface O<sub>3</sub>. The differences between O3CPL\_FIRE and  
239 O3CPL\_NOFIRE, named O3CPL, represent both direct and indirect contributions of  
240 fires to surface O<sub>3</sub>. The differences between O3CPL and O3OFF represent the indirect  
241 contributions of fires to surface O<sub>3</sub> through O<sub>3</sub>-vegetation interactions.



242

## 243 **3 Results**

### 244 **3.1 Model validation**

245 Simulated surface daily maximum 8-hour average O<sub>3</sub> concentrations (MDA8 [O<sub>3</sub>],  
246 short for [O<sub>3</sub>] hereafter) are evaluated using measurements from the AQS and EMEP  
247 datasets over the period of 2005-2012 (Fig 2). The model well captures the observed  
248 spatial distribution of annual [O<sub>3</sub>] in the U.S. and Europe, with a high correlation  
249 coefficient of 0.51 (p<0.01). Although GC-YIBs overestimates the [O<sub>3</sub>] in the eastern  
250 U.S. while underestimating it in western Europe, the normalized mean bias (NMB) is  
251 only 4.0%, with a root mean square error (RMSE) of 5.4 ppbv. Therefore, the  
252 simulated O<sub>3</sub> vegetation damage in our study is slightly overestimated in the eastern  
253 U.S. but underestimated in western Europe.

254

### 255 **3.2 Direct contributions of fires to O<sub>3</sub>**

256 Without fire emissions, the simulated global mean annual [O<sub>3</sub>] is 23.9 ppbv, with a  
257 grid maximum of 63.7 ppbv over the Beijing–Tianjin–Hebei region averaged for  
258 2005-2012 (Fig. 3a). Most high [O<sub>3</sub>] is distributed in the Northern Hemisphere, where  
259 anthropogenic emissions make the dominant contributions. The inclusion of fire  
260 emissions increases global annual [O<sub>3</sub>] by an average of 1.2 ppbv (5.0%). Regionally,  
261 the largest enhancement of [O<sub>3</sub>] by 5.9 ppbv (24.4%) is averaged over central Africa,  
262 with smaller enhancements of 5.7 ppbv (38.2%) averaged over the Amazon, and 3.8  
263 ppbv (10.2%) averaged over southern Asia. Smaller enhancements of 1.1 ppbv (2.2%),



264 0.9 ppbv (2.1%), and 0.8 ppbv (2.2%) are averaged respectively over eastern China,  
265 western Europe, and the eastern U.S. (Fig. 3b). The predicted fire-induced  
266 enhancements in  $[O_3]$  agree well with the simulations using the same model but with  
267 fire emissions from the Global Fire Emission Database (GFED) version 3 (Yue and  
268 Unger, 2018).

269

270 We further evaluated the model performance in simulating fire-induced  $\Delta[O_3]$  at three  
271 sites across biomass burning regions (Fig. S1). Without fire emissions, the  $[O_3]$  is  
272 obviously underestimated, with NMBs of -25.5% at Tg Malim, -53.6% at Manaus,  
273 and -21.3% at Welgegund. As a comparison, simulations with fire emissions show  
274 NMBs in fire seasons of -8.7% at Tg Malim, -1.4% at Manaus, and -15.1% at  
275 Welgegund, suggesting improved  $O_3$  simulations by including fire emissions.

276

### 277 **3.3 Fire-induced $O_3$ damages to GPP**

278 Surface  $O_3$  causes strong damage to ecosystem productivity (Fig. 4). Without fire  
279 emissions, surface  $O_3$  reduces global annual GPP by 1.7% (3899.8 Tg C yr<sup>-1</sup>, Figs. 4a  
280 and 4c). Regional maximum reductions of 10.9% (372.0 Tg C yr<sup>-1</sup>), 6.1% (366.1 Tg C  
281 yr<sup>-1</sup>), and 4.9% (323.8 Tg C yr<sup>-1</sup>) are averaged respectively over eastern China, the  
282 eastern U.S., and western Europe; these reductions are attributed to the high ambient  
283  $[O_3]$  level and the large stomatal conductance over these regions. The patterns of  
284  $O_3$ -induced GPP reductions agree with previous estimates using different models  
285 (Sitch et al., 2007; Yue and Unger, 2015). The inclusion of fire emissions causes



286 additional GPP reductions. Globally, fire-induced  $\Delta\text{O}_3$  decreases annual GPP by 0.4%  
287 (1312.0 Tg C yr<sup>-1</sup>, Figs. 4b and 4d). Regionally, the largest GPP reduction of 1.4%  
288 (370.3 Tg C yr<sup>-1</sup>) is averaged over the Amazon due to the largest enhancement of  $[\text{O}_3]$   
289 caused by fires. Furthermore, fire  $\Delta[\text{O}_3]$  causes additional annual GPP reductions of  
290 1.3% (358.0 Tg C yr<sup>-1</sup>), averaged over central Africa, and 1.0% (77.1 Tg C yr<sup>-1</sup>),  
291 averaged over southern Asia. In contrast, limited damage is found in eastern China,  
292 western Europe, and the eastern U.S. due to low fire  $\Delta[\text{O}_3]$ . Following the changes in  
293 GPP, fire-induced  $\text{O}_3$  damage to LAI shows a regional maximum of 0.3-0.7% in  
294 central Africa and a global reduction of 0.02-0.5% (Fig. S2).

295

### 296 **3.4 Indirect contributions of fires to $\text{O}_3$**

297 Vegetation parameters such as LAI and stomatal conductance play important roles in  
298 modulating surface  $[\text{O}_3]$ . The  $\text{O}_3$ -induced changes in these variables interactively feed  
299 back to alter local  $[\text{O}_3]$  (Fig. 5). Without fire emissions, the annual  $\Delta[\text{O}_3]$  from  
300  $\text{O}_3$ -vegetation interactions is limited to eastern China by 0.5 ppbv, the eastern U.S. by  
301 0.3 ppbv, and western Europe by 0.2 ppbv. The largest grid positive feedback of up to  
302 0.8 ppbv is found in the eastern U.S. (Figs. 5a and 5c). Sensitivity experiments further  
303 show that such enhancement of surface  $[\text{O}_3]$  mainly results from the inhibition of  
304 stomatal conductance by  $\text{O}_3$  stomatal uptake (Fig. S3a), which reduces the  $\text{O}_3$  dry  
305 deposition velocity (Fig. S4). Consequently, large  $\Delta[\text{O}_3]$  (Figs. 5a and 5c) are  
306 collocated with areas enduring high levels of  $\text{O}_3$  vegetation damage (Figs. 4a and 4c).  
307 As a comparison, the feedback of LAI changes is generally small (Fig. S3b), which is



308 mainly attributed to limited  $O_3$  damage on LAI (Fig. S2). The enhancement of  $[O_3]$   
309 from fires causes additional feedback to the surface  $[O_3]$ . The largest annual  $\Delta[O_3]$  of  
310 0.13 ppbv due to  $O_3$ -vegetation feedback is averaged on over the Amazon (Figs. 5b  
311 and 5d), where the highest GPP reductions by fire-induced  $O_3$  are predicted (Figs. 4b  
312 and 4d). Such feedback additionally enhances local  $[O_3]$  by 0.12 ppbv, averaged over  
313 central Africa, and 0.09 ppbv, averaged over southern Asia. However, limited  
314  $O_3$ -vegetation feedback is found in the eastern U.S., eastern China, and western  
315 Europe, either because of low fire-induced  $\Delta[O_3]$  (Fig. 3b) or low  $\Delta$ GPP (Figs. 4b and  
316 4d). The changes in  $O_3$  dry deposition velocity broadly match the pattern of  
317  $O_3$ -vegetation feedback (Fig. S4), suggesting that reduced dry deposition velocity due  
318 to  $O_3$ -induced inhibition of stomatal conductance is the dominant driver for the  
319 enhanced surface  $[O_3]$ .

320

321 Fig. 6 shows seasonal variations in  $O_3$ -vegetation feedback. Without fire emissions,  
322  $O_3$ -vegetation feedback in eastern China, the eastern U.S., and western Europe shows  
323 similar seasonal variations, increasing from January to July and then decreasing (Fig.  
324 6a). For these regions, surface  $[O_3]$  and stomatal conductance reach maximums during  
325 the growth season (May-October), resulting in instantaneous  $O_3$  uptake. Therefore,  
326  $O_3$ -vegetation interactions are expected to be stronger during the growth season in the  
327 Northern Hemisphere. However,  $O_3$ -vegetation feedback driven by fires in the  
328 Amazon and Southern Asia reaches a maximum during August-December and  
329 February-June, respectively. Moreover, double peaks are shown in central Africa, with



330 maximums during February-April and July-September (Fig. 6b). The distinct seasonal  
331 variations in biomass burning regions are attributed to fire emissions. At low latitudes,  
332 stomatal conductance shows limited seasonal variations. Therefore, O<sub>3</sub>-vegetation  
333 feedback driven by fires is mainly dependent on fire-induced  $\Delta[\text{O}_3]$ .

334

335 Fire-induced O<sub>3</sub> shows stronger interactions with vegetation under favorable  
336 meteorological conditions. We sort daily  $\Delta[\text{O}_3]$  from O<sub>3</sub>-vegetation feedback and  
337 calculate the average of  $\Delta[\text{O}_3]$  above the 95<sup>th</sup> percentile (Fig. S5). The spatial pattern  
338 of  $\Delta[\text{O}_3]$  during extreme O<sub>3</sub>-vegetation feedback is broadly consistent with that of the  
339 annual average, albeit with much stronger O<sub>3</sub>-vegetation feedback. Without fire  
340 emissions, O<sub>3</sub>-vegetation feedback enhances [O<sub>3</sub>] by 2.0 ppbv averaged over eastern  
341 China, 1.8 ppbv averaged over the eastern U.S., and 1.1 ppbv averaged over western  
342 Europe (Figs. S5a and S5c). Fire emissions alone enhance [O<sub>3</sub>] through O<sub>3</sub>-vegetation  
343 interactions by 1.1 ppbv averaged over the Amazon, 0.8 ppbv averaged over southern  
344 Asia, and 0.6 ppbv averaged over central Africa during extreme O<sub>3</sub>-vegetation  
345 feedback (Figs. S5b and S5d).

346

### 347 **3.5 Indirect vs. direct contributions of fires to O<sub>3</sub>**

348 We further compare the indirect and direct contributions of fire emissions to surface  
349 [O<sub>3</sub>]. Here, the direct contributions indicate  $\Delta[\text{O}_3]$  caused by fire emissions of  
350 chemical precursors, while the indirect contributions represent additional  $\Delta[\text{O}_3]$  from  
351 O<sub>3</sub>-vegetation interactions caused by fire-induced O<sub>3</sub>. Without fire emissions,





352 O<sub>3</sub>-vegetation interactions cause enhancement of [O<sub>3</sub>] by 1.0% averaged over eastern  
353 China, 0.8% averaged over the eastern U.S., and 0.5% averaged over western Europe  
354 (Figs. 7a and 7c). Compared to nonfire sources, fire emissions cause larger  
355 perturbations in surface [O<sub>3</sub>] through O<sub>3</sub>-vegetation interactions (Figs. 7b and 7d). The  
356 ratios of indirect to direct annual  $\Delta$ [O<sub>3</sub>] are 3.7% averaged over eastern China, 2.0%  
357 averaged over the eastern U.S., and 1.6% averaged over western Europe. For these  
358 regions, the absolute  $\Delta$ [O<sub>3</sub>] from direct fire emissions is usually lower than 1 ppbv  
359 (Fig. 3b). However, the high level of ambient [O<sub>3</sub>] (Fig. 3a) provides a sensitive  
360 environment in which moderate increases in [O<sub>3</sub>] from fires can cause large indirect  
361 contributions to regional [O<sub>3</sub>] through vegetation damage. For fire-prone regions, the  
362 ratios of indirect to direct annual  $\Delta$ [O<sub>3</sub>] are 2.6% averaged over southern Asia, 1.9%  
363 averaged over the eastern U.S., and 1.4% averaged over central Africa.

364

### 365 **3.6 Aggravated O<sub>3</sub> damage to GPP through O<sub>3</sub>-vegetation feedback**

366 The additional O<sub>3</sub> enhancement can exacerbate the damaging effects on vegetation.  
367 Without fire emissions, online O<sub>3</sub> causes a global annual GPP reduction of 0.2%  
368 (299.6 Tg C yr<sup>-1</sup>, Figs. S6a and S6c) from the offline O<sub>3</sub>. Regionally, additional  
369 reductions are mainly found in eastern China, the eastern U.S., and western Europe,  
370 where GPP is further decreased by 27.1 Tg C yr<sup>-1</sup>, 40.8 Tg C yr<sup>-1</sup> and 28.4 Tg C yr<sup>-1</sup>,  
371 respectively. For fire emissions, the online fire-induced  $\Delta$ O<sub>3</sub> results in a higher GPP  
372 reduction by 25.0 Tg C yr<sup>-1</sup> averaged over the Amazon, and 24.3 Tg C yr<sup>-1</sup> averaged  
373 over central Africa, and 7.1 Tg C yr<sup>-1</sup> averaged over southern Asia compared to the



374 offline fire-induced  $\Delta O_3$  (Figs. S6b and S6d). Such spatial patterns are broadly  
375 consistent with  $\Delta[O_3]$  induced by  $O_3$ -vegetation feedback (Fig. 5).

376

#### 377 **4 Conclusions and discussion**

378 Many studies have explored the direct contributions to surface  $O_3$  by fire emissions.  
379 However, the feedback of fire-induced  $O_3$  vegetation damage to surface  $[O_3]$  remains  
380 unquantified. In this study, we find that fire-induced  $O_3$  causes a positive feedback to  
381 surface  $[O_3]$  mainly because of the inhibition effects on stomatal conductance.  
382 Regionally,  $O_3$ -vegetation feedback driven by fires enhances surface annual  $[O_3]$  by  
383 0.13 ppbv averaged over the Amazon, 0.12 ppbv averaged over central Africa, and  
384 0.09 ppbv averaged over southern Asia. Such feedback exhibit large seasonal  
385 variations, with the maximums of 0.5 ppbv averaged over the Amazon in October, 0.3  
386 ppbv averaged over southern Asia in April, and 0.2 ppbv averaged over central Africa  
387 in April. During extreme  $O_3$ -vegetation interactions, the feedback can rise to  $>0.6$   
388 ppbv in these fire-prone areas. Although direct formations of  $O_3$  from fires are limited  
389 in eastern China and the eastern U.S., the feedback of  $O_3$ -vegetation coupling results  
390 in additional enhancement of surface  $[O_3]$  by 3.7% and 2.0% upon the fire-induced  
391  $\Delta[O_3]$ . Such large ratios in these regions are attributed to the high level of ambient  $[O_3]$   
392 that provides a sensitive environment in which moderate increases in  $[O_3]$  from fires  
393 can cause large indirect contributions to regional  $[O_3]$  through vegetation damage.

394

395 Some uncertainties may affect the conclusions of this study. First, we employed a



396 model resolution of  $4^{\circ}\times 5^{\circ}$  due to the limitations in computational resources. We  
397 performed a one-year sensitivity simulation at a  $2^{\circ}\times 2.5^{\circ}$  resolution. The comparisons  
398 show that fire-induced direct  $O_3$  enhancement is very similar between the simulations  
399 with low and high resolutions, although the former runs predict slightly higher  
400 changes in  $[O_3]$  than the latter (Fig. S7). Second, different biomass burning datasets  
401 may affect the estimated  $O_3$ -vegetation feedback in our study. At present, the  
402 FINNv1.5 and GFEDv4.1 inventories are available in the public-release of  
403 GEOS-Chem v12.0.0. Compared with the FINNv1.5 inventory, simulations using the  
404 GFEDv4.1 inventory predict a lower  $O_3$ -vegetation feedback in the Amazon (Fig. S8a)  
405 and southern Asia (Fig. S8c) but a higher  $O_3$ -vegetation feedback in central Africa  
406 (Fig. S8b). Finally, fires can decrease VOC emissions from biogenic sources by  
407 burning vegetation. However, compared to the VOCs emitted by fires, the VOC loss  
408 from burned vegetation is generally smaller (Fig. S9). Therefore, the influence of  
409 reduced VOCs from vegetation loss on surface  $[O_3]$  can be ignored.

410

411 Despite these uncertainties, we present the first estimate of  $O_3$  enhancement by fire  
412 emissions through  $O_3$ -vegetation interactions. Such enhancement is not limited to  
413 fire-prone regions, but is also significant over downwind areas with high ambient  $[O_3]$   
414 levels. Although the absolute perturbations may be moderate for the whole fire season,  
415  $O_3$ -vegetation interactions can largely increase surface  $O_3$  during extreme  
416  $O_3$ -vegetation interactions, leading to additional threats to public health and  
417 ecosystem productivity.



418

419 **Data availability**

420 The site-level [O<sub>3</sub>] in the U.S. can be download from AQS (<https://www.epa.gov/aqs>).

421 The site-level [O<sub>3</sub>] in the Europe can be download from EMEP (<https://emep.int>). The  
422 observed [O<sub>3</sub>] at Manaus, Tg Malim, and Welgegund sites are from earlier studies  
423 (Ahamad et al., 2014; Laban et al., 2018; Pope et al., 2020). The GC-YIBs simulation  
424 results are available from the corresponding authors on request.

425

426 **Competing interests.** The authors declare no competing financial interests.

427

428 **Author Contributions.** XY conceived the study. YL conducted the model  
429 simulations. YL and XY were responsible for results analysis. HL, LZ, and YY  
430 revised and improved the manuscript. HZ, CT, and CG helped prepare model input.  
431 YM, LG, and YC helped prepare observation dataset.

432

433 **Acknowledgements.** This work was supported by Jiangsu Science Fund for  
434 Distinguished Young Scholars (grant no. BK20200040), the National Natural Science  
435 Foundation of China (grant no. 41975155), and the National Key Research and  
436 Development Program of China (grant nos. 2019YFA0606802 and  
437 2017YFA0603802).

438

439



## 440 References

- 441 Ahamad, F., Latif, M. T., Tang, R., Juneng, L., Dominick, D., and Juahir, H.: Variation of surface ozone  
442 exceedance around Klang Valley, Malaysia, *Atmospheric research*, 139, 116-127, 2014.
- 443 Ainsworth, E. A., Yendrek, C. R., Sitch, S., Collins, W. J., and Emberson, L. D.: The Effects of  
444 Tropospheric Ozone on Net Primary Productivity and Implications for Climate Change, *Annu Rev*  
445 *Plant Biol*, 63, 637-661, 2012.
- 446 Akagi, S., Yokelson, R. J., Wiedinmyer, C., Alvarado, M., Reid, J., Karl, T., Crouse, J., and Wennberg,  
447 P.: Emission factors for open and domestic biomass burning for use in atmospheric models, *Atmos*  
448 *Chem Phys*, 11, 4039-4072, 2011.
- 449 Akhtar, N., Yamaguchi, M., Inada, H., Hoshino, D., Kondo, T., and Izuta, T.: Effects of ozone on  
450 growth, yield and leaf gas exchange rates of two Bangladeshi cultivars of wheat (*Triticum aestivum* L.),  
451 *Environ Pollut*, 158, 1763-1767, 2010.
- 452 Amiro, B. D., Cantin, A., Flannigan, M. D., and de Groot, W. J.: Future emissions from Canadian  
453 boreal forest fires, *Can J Forest Res*, 39, 383-395, 2009.
- 454 Andreae, M. and Rosenfeld, D.: Aerosol–cloud–precipitation interactions. Part 1. The nature and  
455 sources of cloud-active aerosols, *Earth-Science Reviews*, 89, 13-41, 2008.
- 456 Andreae, M. O. and Merlet, P.: Emission of trace gases and aerosols from biomass burning, *Global*  
457 *biogeochemical cycles*, 15, 955-966, 2001.
- 458 Baldocchi, D. D., Hicks, B. B., and Camara, P.: A Canopy Stomatal-Resistance Model for Gaseous  
459 Deposition to Vegetated Surfaces, *Atmospheric Environment*, 21, 91-101, 1987.
- 460 Balshi, M. S., McGuire, A. D., Duffy, P., Flannigan, M., Walsh, J., and Melillo, J.: Assessing the  
461 response of area burned to changing climate in western boreal North America using a Multivariate  
462 Adaptive Regression Splines (MARS) approach, *Global Change Biol*, 15, 578-600, 2009.
- 463 Barret, B., Sauvage, B., Bennouna, Y., and Le Flochmoen, E.: Upper-tropospheric CO and O<sub>3</sub> budget  
464 during the Asian summer monsoon, *Atmos. Chem. Phys*, 16, 9129-9147, 2016.
- 465 Bey, I., Jacob, D. J., Logan, J. A., and Yantosca, R. M.: Asian chemical outflow to the Pacific in spring:  
466 Origins, pathways, and budgets, *J Geophys Res-Atmos*, 106, 23097-23113, 2001.
- 467 Bond-Lamberty, B., Peckham, S. D., Ahl, D. E., and Gower, S. T.: Fire as the dominant driver of  
468 central Canadian boreal forest carbon balance, *Nature*, 450, 89-92, 2007.
- 469 Booker, F. L., Burkey, K. O., Pursley, W. A., and Heagle, A. S.: Elevated carbon dioxide and ozone  
470 effects on peanut: I. Gas-exchange, biomass, and leaf chemistry, *Crop Sci*, 47, 1475-1487, 2007.
- 471 Brey, S. J., Barnes, E. A., Pierce, J. R., Wiedinmyer, C., and Fischer, E. V.: Environmental Conditions,  
472 Ignition Type, and Air Quality Impacts of Wildfires in the Southeastern and Western United States,  
473 *Earth's Future*, 6, 1442-1456, 2018.
- 474 Cheng, L., McDonald, K. M., Angle, R. P., and Sandhu, H. S.: Forest fire enhanced photochemical air  
475 pollution. A case study, *Atmospheric Environment*, 32, 673-681, 1998.
- 476 Clark, D., Mercado, L., Sitch, S., Jones, C., Gedney, N., Best, M., Pryor, M., Rooney, G., Essery, R.,  
477 and Blyth, E.: The Joint UK Land Environment Simulator (JULES), model description—Part 2: carbon  
478 fluxes and vegetation dynamics, *Geosci Model Dev*, 4, 701-722, 2011.
- 479 Curci, G., Beekmann, M., Vautard, R., Smiatek, G., Steinbrecher, R., Theloke, J., and Friedrich, R.:  
480 Modelling study of the impact of isoprene and terpene biogenic emissions on European ozone levels,  
481 *Atmospheric Environment*, 43, 1444-1455, 2009.
- 482 Dang, R. and Liao, H.: Severe winter haze days in the Beijing–Tianjin–Hebei region from 1985 to 2017



- 483 and the roles of anthropogenic emissions and meteorology, *Atmos Chem Phys*, 19, 10801-10816, 2019.
- 484 David, L. M., Ravishankara, A., Brewer, J. F., Sauvage, B., Thouret, V., Venkataramani, S., and Sinha,
- 485 V.: Tropospheric ozone over the Indian subcontinent from 2000 to 2015: Data set and simulation using
- 486 GEOS-Chem chemical transport model, *Atmospheric Environment*, 219, 117039, 2019.
- 487 Farquhar, G. D., von Caemmerer, S. v., and Berry, J. A.: A biochemical model of photosynthetic CO<sub>2</sub>
- 488 assimilation in leaves of C<sub>3</sub> species, *Planta*, 149, 78-90, 1980.
- 489 Fitzky, A. C., Sandén, H., Karl, T., Fares, S., Calfapietra, C., Grote, R., Saunier, A., and Rewald, B.:
- 490 The interplay between ozone and urban vegetation–BVOC emissions, ozone deposition and tree
- 491 ecophysiology, *Frontiers in Forests and Global Change*, 2, 50, 2019.
- 492 Fountoukis, C. and Nenes, A.: ISORROPIA II: a computationally efficient thermodynamic equilibrium
- 493 model for K<sup>+</sup>-Ca<sup>2+</sup>-Mg<sup>2+</sup>-NH<sub>4</sub><sup>+</sup>-Na<sup>+</sup>-SO<sub>4</sub><sup>2-</sup> NO<sub>3</sub><sup>-</sup>-Cl<sup>-</sup>-H<sub>2</sub>O aerosols, *Atmos Chem Phys*, 7, 4639-4659,
- 494 2007.
- 495 Fowler, D., Pilegaard, K., Sutton, M. A., Ambus, P., Raivonen, M., Duyzer, J., Simpson, D., Fagerli, H.,
- 496 Fuzzi, S., Schjoerring, J. K., Granier, C., Neftel, A., Isaksen, I. S. A., Laj, P., Maione, M., Monks, P. S.,
- 497 Burkhardt, J., Daemmgen, U., Neirynek, J., Personne, E., Wichink-Kruit, R., Butterbach-Bahl, K.,
- 498 Flechard, C., Tuovinen, J. P., Coyle, M., Gerosa, G., Loubet, B., Altimir, N., Gruenhage, L., Ammann,
- 499 C., Cieslik, S., Paoletti, E., Mikkelsen, T. N., Ro-Poulsen, H., Cellier, P., Cape, J. N., Horvath, L.,
- 500 Loreto, F., Niinemets, U., Palmer, P. I., Rinne, J., Misztal, P., Nemitz, E., Nilsson, D., Pryor, S.,
- 501 Gallagher, M. W., Vesala, T., Skiba, U., Brüeggemann, N., Zechmeister-Boltenstern, S., Williams, J.,
- 502 O'Dowd, C., Facchini, M. C., de Leeuw, G., Flossman, A., Chaumerliac, N., and Erisman, J. W.:
- 503 Atmospheric composition change: Ecosystems-Atmosphere interactions, *Atmospheric Environment*, 43,
- 504 5193-5267, 2009.
- 505 Gong, C., Lei, Y., Ma, Y., Yue, X., and Liao, H.: Ozone-vegetation feedback through dry deposition and
- 506 isoprene emissions in a global chemistry-carbon-climate model, *Atmos Chem Phys*, 20, 3841-3857,
- 507 2020.
- 508 Gong, C. and Liao, H.: A typical weather pattern for ozone pollution events in North China, *Atmos*
- 509 *Chem Phys*, 19, 13725-13740, 2019.
- 510 He, C., Clifton, O., and Coauthors: Interactions between Air Pollution and Terrestrial Ecosystems:
- 511 Perspectives on Challenges and Future Directions, *Bulletin of the American Meteorological Society*,
- 512 doi: doi: <https://doi.org/10.1175/BAMS-D-20-0066.1>, 2020. 2020.
- 513 Heald, C. L. and Geddes, J. A.: The impact of historical land use change from 1850 to 2000 on
- 514 secondary particulate matter and ozone, *Atmos Chem Phys*, 16, 14997-15010, 2016.
- 515 Inada, H., Kondo, T., Akhtar, N., Hoshino, D., Yamaguchi, M., and Izuta, T.: Relationship between
- 516 cultivar difference in the sensitivity of net photosynthesis to ozone and reactive oxygen species
- 517 scavenging system in Japanese winter wheat (*Triticum aestivum*), *Physiol Plantarum*, 146, 217-227,
- 518 2012.
- 519 Jaffe, D., Bertschi, I., Jaegle, L., Novelli, P., Reid, J. S., Tanimoto, H., Vingarzan, R., and Westphal, D.
- 520 L.: Long-range transport of Siberian biomass burning emissions and impact on surface ozone in
- 521 western North America, *Geophys Res Lett*, 31, 2004.
- 522 Jaffe, D. A., Wigder, N., Downey, N., Pfister, G., Boynard, A., and Reid, S. B.: Impact of wildfires on
- 523 ozone exceptional events in the Western US, *Environ Sci Technol*, 47, 11065-11072, 2013.
- 524 Jaffe, D. A. and Wigder, N. L.: Ozone production from wildfires: A critical review, *Atmospheric*
- 525 *Environment*, 51, 1-10, 2012.
- 526 Jiang, X. Y., Wiedinmyer, C., and Carlton, A. G.: Aerosols from Fires: An Examination of the Effects



- 527 on Ozone Photochemistry in the Western United States, *Environmental Science & Technology*, 46,  
528 11878-11886, 2012.
- 529 Karnosky, D. F., Skelly, J. M., Percy, K. E., and Chappelka, A. H.: Perspectives regarding 50 years of  
530 research on effects of tropospheric ozone air pollution on US forests, *Environ Pollut*, 147, 489-506,  
531 2007.
- 532 Keller, C. A., Long, M. S., Yantosca, R. M., Da Silva, A., Pawson, S., and Jacob, D. J.: HEMCO v1. 0:  
533 a versatile, ESMF-compliant component for calculating emissions in atmospheric models, *Geosci.*  
534 *Model Dev.*, 7, 1409-1417, 2014.
- 535 Kita, K., Fujiwara, M., and Kawakami, S.: Total ozone increase associated with forest fires over the  
536 Indonesian region and its relation to the El Nino-Southern oscillation, *Atmospheric Environment*, 34,  
537 2681-2690, 2000.
- 538 Laban, T. L., Van Zyl, P. G., Beukes, J. P., Vakkari, V., Jaars, K., Borduas-Dedekind, N., Josipovic, M.,  
539 Thompson, A. M., Kulmala, M., and Laakso, L.: Seasonal influences on surface ozone variability in  
540 continental South Africa and implications for air quality, *Atmos Chem Phys*, 18, 15491-15514, 2018.
- 541 Larsen, A. E., Reich, B. J., Ruminiski, M., and Rappold, A. G.: Impacts of fire smoke plumes on  
542 regional air quality, 2006-2013, *J Expo Sci Env Epid*, 28, 319-327, 2018.
- 543 Lei, Y., Yue, X., Liao, H., Gong, C., and Zhang, L.: Implementation of Yale Interactive terrestrial  
544 Biosphere model v1.0 into GEOS-Chem v12.0.0: a tool for biosphere-chemistry interactions, *Geosci*  
545 *Model Dev*, 13, 1137-1153, 2020.
- 546 Li, S., Chen, L., Huang, G., Lin, J., Yan, Y., Ni, R., Huo, Y., Wang, J., Liu, M., and Weng, H.: Retrieval  
547 of surface PM<sub>2.5</sub> mass concentrations over North China using visibility measurements and  
548 GEOS-Chem simulations, *Atmospheric Environment*, 2019. 117121, 2019.
- 549 Lin, M., Malyshev, S., Shevliakova, E., Paulot, F., Horowitz, L. W., Fares, S., Mikkelsen, T. N., and  
550 Zhang, L.: Sensitivity of Ozone Dry Deposition to Ecosystem-Atmosphere Interactions: A Critical  
551 Appraisal of Observations and Simulations, *Global Biogeochemical Cycles*, 33, 1264-1288, 2019.
- 552 Lu, X., Zhang, L., Chen, Y., Zhou, M., Zheng, B., Li, K., Liu, Y., Lin, J., Fu, T.-M., and Zhang, Q.:  
553 Exploring 2016-2017 surface ozone pollution over China: source contributions and meteorological  
554 influences, *Atmos Chem Phys*, 19, 8339-8361, 2019.
- 555 Lu, X., Zhang, L., Yue, X., Zhang, J., Jaffe, D. A., Stohl, A., Zhao, Y., and Shao, J.: Wildfire influences  
556 on the variability and trend of summer surface ozone in the mountainous western United States, *Atmos*  
557 *Chem Phys*, 16, 14687-14702, 2016.
- 558 Manninen, S., Siivonen, N., Timonen, U., and Huttunen, S.: Differences in ozone response between  
559 two Finnish wild strawberry populations, *Environ Exp Bot*, 49, 29-39, 2003.
- 560 Martin, M. V., Honrath, R., Owen, R. C., Pfister, G., Fialho, P., and Barata, F.: Significant  
561 enhancements of nitrogen oxides, black carbon, and ozone in the North Atlantic lower free troposphere  
562 resulting from North American boreal wildfires, *Journal of Geophysical Research: Atmospheres*, 111,  
563 D23S60, 2006.
- 564 McKeen, S. A., Wotawa, G., Parrish, D. D., Holloway, J. S., Buhr, M. P., Hubler, G., C., F. F., and  
565 Meagher, J. F.: Ozone production from Canadian wildfires during June and July of 1995, *Journal of*  
566 *Geophysical Research*, 107, 4192, 2002.
- 567 McLinden, C., Olsen, S., Hannegan, B., Wild, O., Prather, M., and Sundet, J.: Stratospheric ozone in  
568 3-D models: A simple chemistry and the cross-tropopause flux, *Journal of Geophysical Research:*  
569 *Atmospheres*, 105, 14653-14665, 2000.
- 570 Nuryanto, D. E.: Simulation of forest fires smoke using WRF-Chem model with FINN fire emissions



- 571 in Sumatera, *Procedia Environ Sci*, 24, 65-69, 2015.
- 572 Oltmans, S. J., Lefohn, A. S., Harris, J. M., Tarasick, D. W., Thompson, A. M., Wernli, H., Johnson, B.  
573 J., Novelli, P. C., Montzka, S. A., Ray, J. D., Patrick, L. C., Sweeney, C., Jefferson, A., Dann, T.,  
574 Davies, J., Shapiro, M., and Holben, B. N.: Enhanced ozone over western North America from biomass  
575 burning in Eurasia during April 2008 as seen in surface and profile observations, *Atmospheric*  
576 *Environment*, 44, 4497-4509, 2010.
- 577 Pfister, G. G., Emmons, L. K., Hess, P. G., Honrath, R., Lamarque, J. F., Martin, M. V., Owen, R. C.,  
578 Avery, M. A., Browell, E. V., Holloway, J. S., Nedelec, P., Purvis, R., Ryerson, T. B., Sachse, G. W.,  
579 and Schlager, H.: Ozone production from the 2004 North American boreal fires, *J Geophys Res-Atmos*,  
580 111, D24S07, 2006.
- 581 Pfister, G. G., Wiedinmyer, C., and Emmons, L. K.: Impacts of the fall 2007 California wildfires on  
582 surface ozone: Integrating local observations with global model simulations, *Geophys Res Lett*, 35,  
583 L19814, 2008.
- 584 Pope, R. J., Arnold, S. R., Chipperfield, M. P., Reddington, C. L., Butt, E. W., Keslake, T. D., Feng, W.,  
585 Latter, B. G., Kerridge, B. J., and Siddans, R.: Substantial increases in Eastern Amazon and Cerrado  
586 biomass burning-sourced tropospheric ozone, *Geophys Res Lett*, 47, e2019GL084143, 2020.
- 587 Sadiq, M., Tai, A. P. K., Lombardozi, D., and Martin, M. V.: Effects of ozone-vegetation coupling on  
588 surface ozone air quality via biogeochemical and meteorological feedbacks, *Atmos Chem Phys*, 17,  
589 3055-3066, 2017.
- 590 Schiferl, L. D. and Heald, C. L.: Particulate matter air pollution may offset ozone damage to global  
591 crop production, *Atmos Chem Phys*, 18, 5953-5966, 2018.
- 592 Singh, H. B., Anderson, B. E., Brune, W. H., Cai, C., Cohen, R. C., Crawford, J. H., Cubison, M. J.,  
593 Czech, E. P., Emmons, L., Fuelberg, H. E., Huey, G., Jacob, D. J., Jimenez, J. L., Kaduwela, A., Kondo,  
594 Y., Mao, J., Olson, J. R., Sachse, G. W., Vay, S. A., Weinheimer, A., Wennberg, P. O., Wisthaler, A., and  
595 Team, A. S.: Pollution influences on atmospheric composition and chemistry at high northern latitudes:  
596 Boreal and California forest fire emissions, *Atmospheric Environment*, 44, 4553-4564, 2010.
- 597 Sitch, S., Cox, P. M., Collins, W. J., and Huntingford, C.: Indirect radiative forcing of climate change  
598 through ozone effects on the land-carbon sink, *Nature*, 448, 791-794, 2007.
- 599 Spitters, C.: Separating the diffuse and direct component of global radiation and its implications for  
600 modeling canopy photosynthesis Part II. Calculation of canopy photosynthesis, *Agricultural and Forest*  
601 *meteorology*, 38, 231-242, 1986.
- 602 Travis, K. R., Jacob, D. J., Fisher, J. A., Kim, P. S., Marais, E. A., Zhu, L., Yu, K., Miller, C. C.,  
603 Yantosca, R. M., and Sulprizio, M. P.: Why do models overestimate surface ozone in the southeastern  
604 United States?, *Atmos Chem Phys*, 16, 13561, 2016.
- 605 Turetsky, M. R., Kane, E. S., Harden, J. W., Ottmar, R. D., Manies, K. L., Hoy, E., and Kasischke, E. S.:  
606 Recent acceleration of biomass burning and carbon losses in Alaskan forests and peatlands, *Nat Geosci*,  
607 4, 27-31, 2011.
- 608 Val Martin, M., Heald, C., and Arnold, S.: Coupling dry deposition to vegetation phenology in the  
609 Community Earth System Model: Implications for the simulation of surface O<sub>3</sub>, *Geophys Res Lett*, 41,  
610 2988-2996, 2014.
- 611 Val Martin, M., Heald, C. L., and Arnold, S. R.: Coupling dry deposition to vegetation phenology in the  
612 Community Earth System Model: Implications for the simulation of surface O<sub>3</sub>, *Geophys Res Lett*, 41,  
613 2988-2996, 2014.
- 614 van der Werf, G. R., Randerson, J. T., Giglio, L., Collatz, G. J., Mu, M., Kasibhatla, P. S., Morton, D.





- 615 C., DeFries, R. S., Jin, Y., and van Leeuwen, T. T.: Global fire emissions and the contribution of  
616 deforestation, savanna, forest, agricultural, and peat fires (1997-2009), *Atmos Chem Phys*, 10,  
617 11707-11735, 2010.
- 618 Von Caemmerer, S. v. and Farquhar, G. D.: Some relationships between the biochemistry of  
619 photosynthesis and the gas exchange of leaves, *Planta*, 153, 376-387, 1981.
- 620 Vongruang, P., Wongwises, P., and Pimonsree, S.: Assessment of fire emission inventories for  
621 simulating particulate matter in Upper Southeast Asia using WRF-CMAQ, *Atmos Pollut Res*, 8,  
622 921-929, 2017.
- 623 Wang, X. L., Parisien, M. A., Taylor, S. W., Perrakis, D. D. B., Little, J., and Flannigan, M. D.: Future  
624 burn probability in south-central British Columbia, *Int J Wildland Fire*, 25, 200-212, 2016.
- 625 Watson, G. L., Telesca, D., Reid, C. E., Pfister, G. G., and Jerrett, M.: Machine learning models  
626 accurately predict ozone exposure during wildfire events, *Environ Pollut*, 254, 112792, 2019.
- 627 Wesely, M. L. and Hicks, B. B.: A review of the current status of knowledge on dry deposition,  
628 *Atmospheric Environment*, 34, 2261-2282, 2000.
- 629 Wiedinmyer, C., Akagi, S. K., Yokelson, R. J., Emmons, L. K., Al-Saadi, J. A., Orlando, J. J., and Soja,  
630 A. J.: The Fire INventory from NCAR (FINN): a high resolution global model to estimate the  
631 emissions from open burning, *Geosci Model Dev*, 4, 625-641, 2011.
- 632 Wittig, V. E., Ainsworth, E. A., Naidu, S. L., Karnosky, D. F., and Long, S. P.: Quantifying the impact  
633 of current and future tropospheric ozone on tree biomass, growth, physiology and biochemistry: a  
634 quantitative meta-analysis, *Global Change Biol*, 15, 396-424, 2009.
- 635 Yan, Y., Lin, J., and He, C.: Ozone trends over the United States at different times of day, *Atmos Chem*  
636 *Phys*, 18, 1185, 2018.
- 637 Yokelson, R. J., Burling, I. R., Urbanski, S. P., Atlas, E. L., Adachi, K., Buseck, P. R., Wiedinmyer, C.,  
638 Akagi, S. K., Toohey, D. W., and Wold, C. E.: Trace gas and particle emissions from open biomass  
639 burning in Mexico, *Atmos Chem Phys*, 11, 6787-6808, 2011.
- 640 Yue, X., Keenan, T. F., Munger, W., and Unger, N.: Limited effect of ozone reductions on the 20-year  
641 photosynthesis trend at Harvard forest, *Global Change Biol*, 22, 3750-3759, 2016.
- 642 Yue, X., Mickley, L., Logan, J., Hudman, R., Martin, M. V., and Yantosca, R.: Impact of 2050 climate  
643 change on North American wildfire: consequences for ozone air quality, *Atmos Chem Phys*, 15,  
644 10033-10055, 2015.
- 645 Yue, X., Strada, S., Unger, N., and Wang, A. H.: Future inhibition of ecosystem productivity by  
646 increasing wildfire pollution over boreal North America, *Atmos Chem Phys*, 17, 13699-13719, 2017.
- 647 Yue, X. and Unger, N.: Fire air pollution reduces global terrestrial productivity, *Nat Commun*, 9, 5413,  
648 2018.
- 649 Yue, X. and Unger, N.: Ozone vegetation damage effects on gross primary productivity in the United  
650 States, *Atmos Chem Phys*, 14, 9137-9153, 2014.
- 651 Yue, X. and Unger, N.: The Yale Interactive terrestrial Biosphere model version 1.0: description,  
652 evaluation and implementation into NASA GISS ModelE2, *Geosci Model Dev*, 8, 2399-2417, 2015.
- 653 Zhang, L., Jacob, D. J., Downey, N. V., Wood, D. A., Blewitt, D., Carouge, C. C., van Donkelaar, A.,  
654 Jones, D. B., Murray, L. T., and Wang, Y.: Improved estimate of the policy-relevant background ozone  
655 in the United States using the GEOS-Chem global model with 1/2×2/3 horizontal resolution over North  
656 America, *Atmospheric Environment*, 45, 6769-6776, 2011.
- 657 Zhou, S. S., Tai, A. P. K., Sun, S. H., Sadiq, M., Heald, C. L., and Geddes, J. A.: Coupling between  
658 surface ozone and leaf area index in a chemical transport model: strength of feedback and implications



659 for ozone air quality and vegetation health, *Atmos Chem Phys*, 18, 14133-14148, 2018.  
660 Ziemke, J. R., Chandra, S., Duncan, B. N., Schoeberl, M. R., Torres, O., Damon, M. R., and Bhartia, P.  
661 K.: Recent biomass burning in the tropics and related changes in tropospheric ozone, *Geophys Res Lett*,  
662 36, L15819, 2009.  
663  
664  
665  
666  
667  
668



669

670 **Table 1** Summary of simulations using the GC-YIBs model

Name	Emissions	O <sub>3</sub> damaging	O <sub>3</sub> sensitivities
CTRL_FIRE_HS	All including fires	Offline	High
CTRL_FIRE_LS	All including fires	Offline	Low
CTRL_NOFIRE_HS	All but without fires	Offline	High
CTRL_NOFIRE_LS	All but without fires	Offline	Low
O3CPL_FIRE_HS	All including fires	Online	High
O3CPL_FIRE_LS	All including fires	Online	Low
O3CPL_NOFIRE_HS	All but without fires	Online	High
O3CPL_NOFIRE_LS	All but without fires	Online	Low

671

672

673

674

675

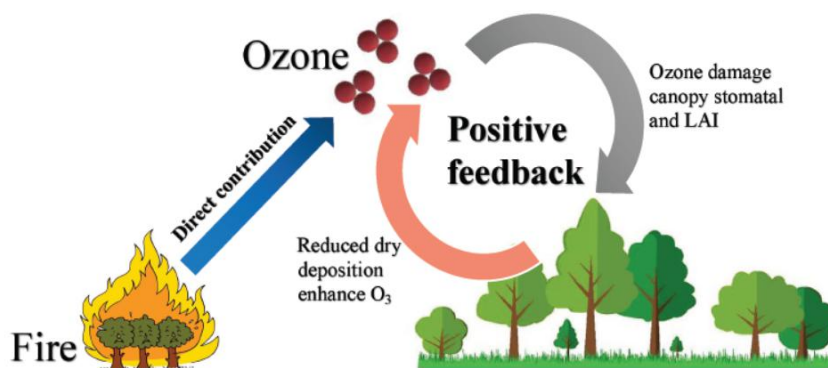
676

677

678

679

680



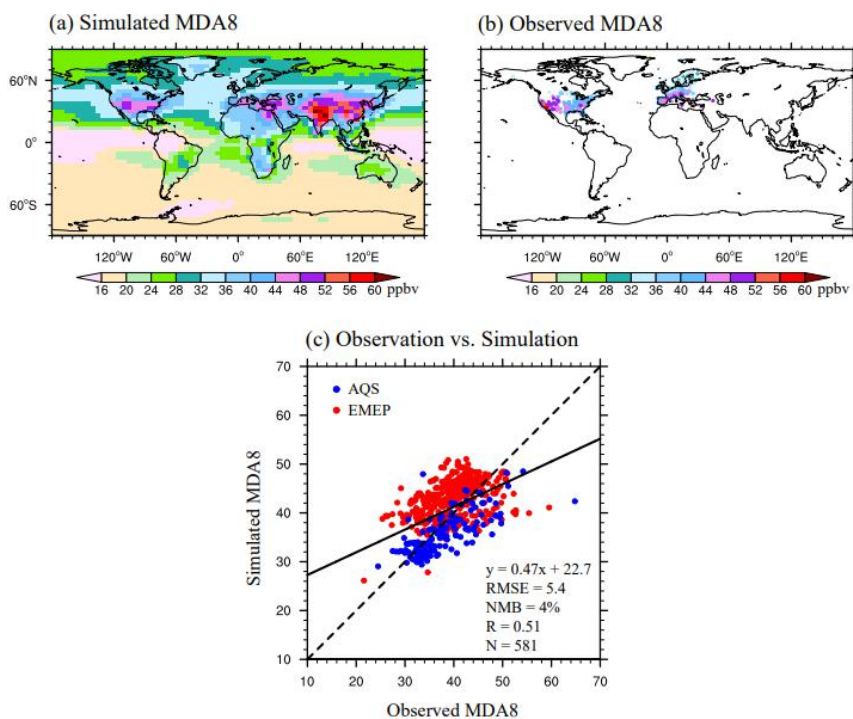
681

682 **Figure 1** Diagram of the impacts of fires on surface O<sub>3</sub> through direct emissions and

683 O<sub>3</sub>-vegetation feedback.

684

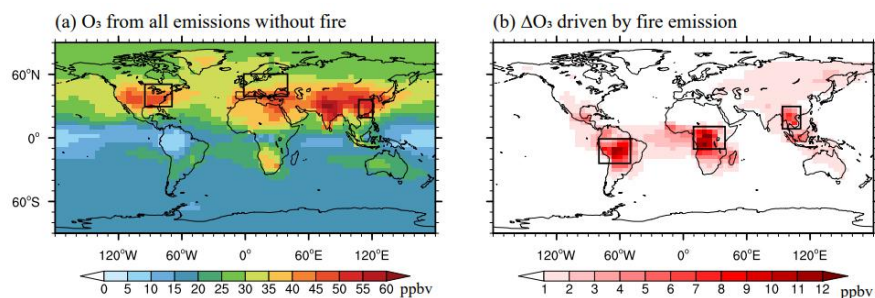
685



686  
687

688 **Figure 2** Spatial pattern of (a) simulated and (b) observed surface  $[O_3]$ . (c) Scatter  
689 plot of surface  $[O_3]$  over measurements in two regions. The black line shows the  
690 linear regression between the observed and simulated  $[O_3]$ . The regression fit,  
691 correlation coefficient (R), root mean square error (RMSE), and normalized mean bias  
692 (NMB) are shown in the bottom panel with an indication of site numbers (N) used for  
693 statistics.

694



695

696 **Figure 3** Annual surface [O<sub>3</sub>] from (a) nonfire and (b) fire-alone sources. The six  
697 subregions are marked with black boxes: Eastern U.S. (EUS, 30°N-50°N,  
698 95°W-70°W), Western Europe (WEU, 40°N-60°N, 0°-40°E), Eastern China (ECH,  
699 20°N-35°N, 108°E-120°E), Amazon (AMZ, 25°S-0°, 80°W-50°W), Central Africa  
700 (CAF, 10°S-10°N, 10°E-40°E), and Southern Asia (SAS, 10°N-30°N, 95°E-110°E).

701

702

703

704

705

706

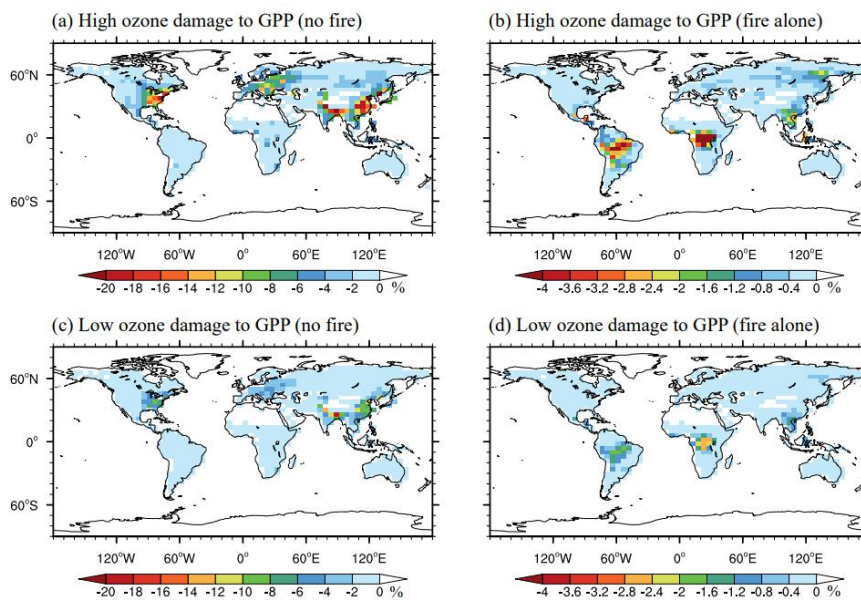
707

708

709

710

711



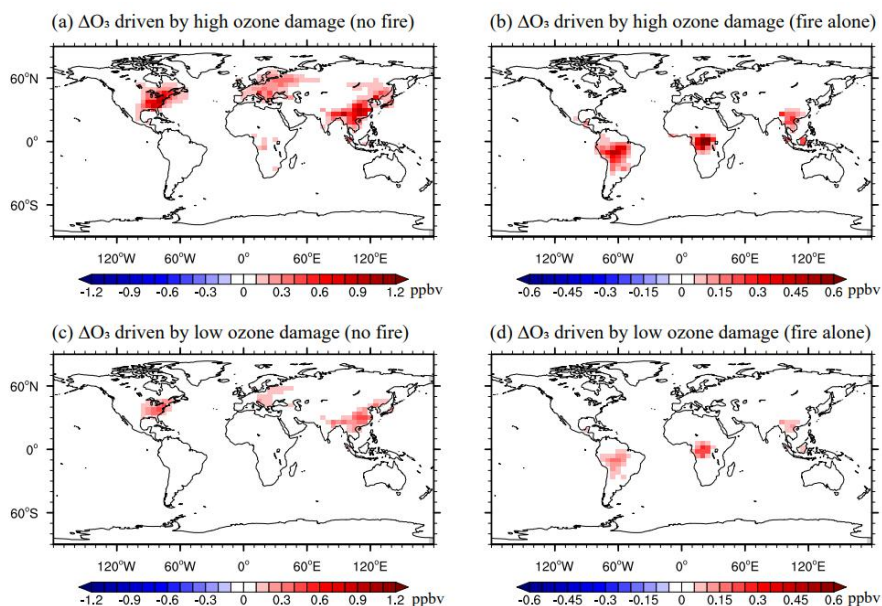
712

713 **Figure 4** Annual percentage of reductions in GPP caused by  $O_3$  from (a, c) nonfire

714 and (b, d) fire alone sources with (a, b) high and (c, d) low  $O_3$  sensitivities. Please

715 note the differences in color scales.

716



717

718 **Figure 5** Annual feedback to surface  $O_3$  caused by  $O_3$  vegetation damage with (a, b)

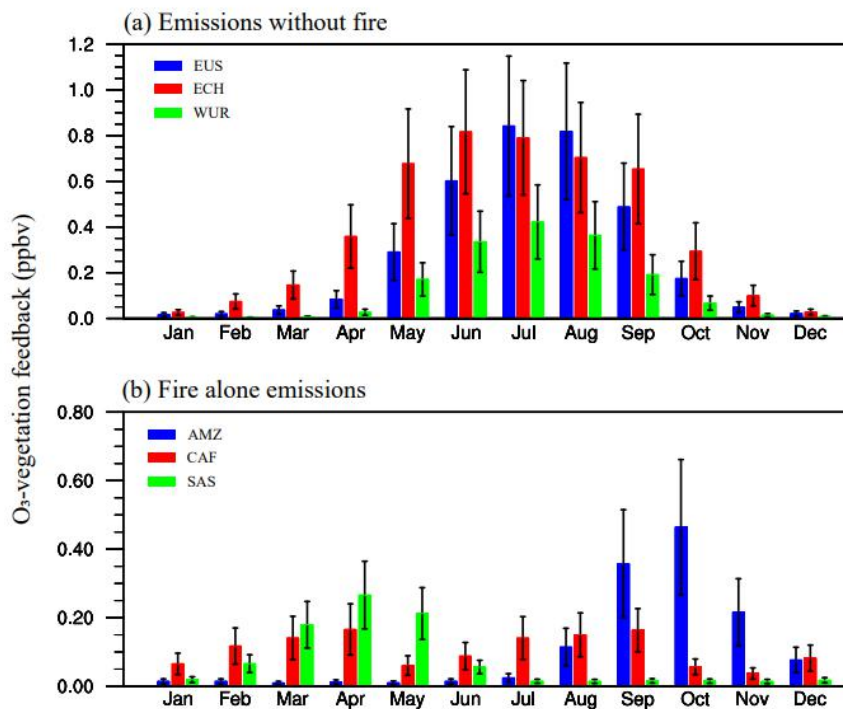
719 high and (c, d) low  $O_3$  sensitivities. (a) and (c) represent feedback by  $O_3$  from nonfire

720 sources; (b) and (d) represent feedback by  $O_3$  from fire emissions alone. Please note

721 the differences in color scales.

722





723

724 **Figure 6** Seasonal variations in O<sub>3</sub>-vegetation feedback driven by (a) nonfire and (b)  
725 fire-alone sources. The error bars represent low to high O<sub>3</sub> damaging sensitivities.

726

727

728

729

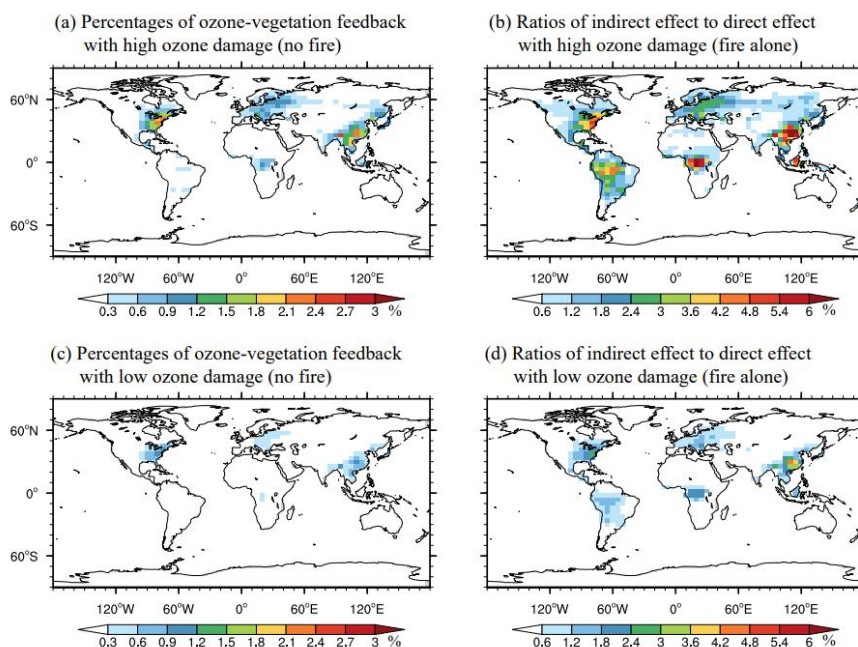
730

731

732

733

734



735

736 **Figure 7** Annal ratios of indirect  $\Delta[\text{O}_3]$  to ambient  $[\text{O}_3]$  from (a, c) nonfire emissions  
737 and the ratios of indirect to direct  $\Delta[\text{O}_3]$  from (b, d) fire emissions alone with (a, b)  
738 high and (c, d) low  $\text{O}_3$  damaging sensitivities. Please note the differences in color  
739 scales.

740

741